A macro-element to simulate 3D soil-structure interaction considering plasticity and uplift

Stéphane Grange, Panagiotis Kotronis, Jacky Mazars

A macro-element to simulate 3D soil-structure interaction considering plasticity and uplift

Stéphane Grange [a,*], Panagiotis Kotronis [a], Jacky Mazars [a]

[a] *Laboratoire 3S-R (Sols, Solides, Structures-Risques) INPG/UJF/CNRS Domaine Universitaire BP 53, 38041 Grenoble cedex 9, France.*

Abstract

In structural engineering, Soil-Structure Interaction (SSI) is an important phenomenon that has to be taken into account. This paper presents a 3D non linear interface element able to compute SSI based on the "macro-element" concept. The particularity of the macro-element lies in the fact that the movement of the foundation is entirely described by a system of generalised variables (forces and displacements) defined at the foundation centre. The non linear behaviour of the soil and the uplift mechanism of the foundation are reproduced using the plasticity theory. The failure surface is defined using an adequate overturning mechanism. Coupling of the different mechanisms is straight forward following the theory of multi-mechanisms. The macro-element is able to simulate the 3D behaviour of a rigid shallow foundation of circular, rectangular or strip shape, submitted to cyclic loadings. It is implemented into FEDEASLab, a finite element MATLAB toolbox. Comparisons with experimental results under cyclic loadings show the performance of the approach.

Key words: Soil-Structure Interaction, Plasticity, Uplift, Macro-element, Shallow foundation

1 Introduction

In the field of earthquake engineering, Soil-Structure Interaction (SSI) is an important phenomenon that has to be taken into account to reproduce correctly the non-linear behaviour of a structure and thus to be able to predict

* Stephane.Grange@hmg.inpg.fr
Email addresses: Panagiotis.Kotronis@hmg.inpg.fr (Panagiotis Kotronis), Jacky.Mazars@inpg.fr (Jacky Mazars).

its relative displacements. Several methods exist: the macro-element approach consists in condensing all non-linearities into a finite domain ("close field") and works with generalised variables (forces and displacements) at the centre of the foundation (figure 1, with $\dot{}$ the symbol of the derivative with respect to time), allowing thus decreasing considerably the necessary degrees of freedom of the numerical model.

Several macro-elements can be found in the literature (Cassidy et al., 2002), (Crémer et al., 2001), (Crémer et al., 2002a), (Crémer et al., 2002b), (di Prisco et al., 2002), (di Prisco et al., 2006), (Martin, 1994), (Nova et al., 1991), (Montrasio et al., 1997), (Paolucci et al., 1997), (Pedretti, 1998), (Tan, 1990). The macro-element presented in (Grange et al., 2008a) reproduces the behaviour of a shallow circular foundation considering the plasticity of the soil. An extension of this macro-element is introduced hereafter for footings of various shapes considering the non linear behaviour of the soil and the uplift of the foundation (Grange, 2008b). Both mechanisms are formulated according to the plasticity theory.

The paper starts with a presentation of the chosen associated dimensionless variables relative to the the different shapes of the footing (circular, rectangular and strip). The 3D elastic, plastic and uplift mechanisms are then presented in detail and their coupling according to the theory of multi-mechanisms. The macro-element is implemented into FEDEASLab, a finite element MATLAB toolbox (Filippou et al., 2004). Numerical results compared with experimental tests under cyclic loadings are provided to show the performance of this new numerical tool.

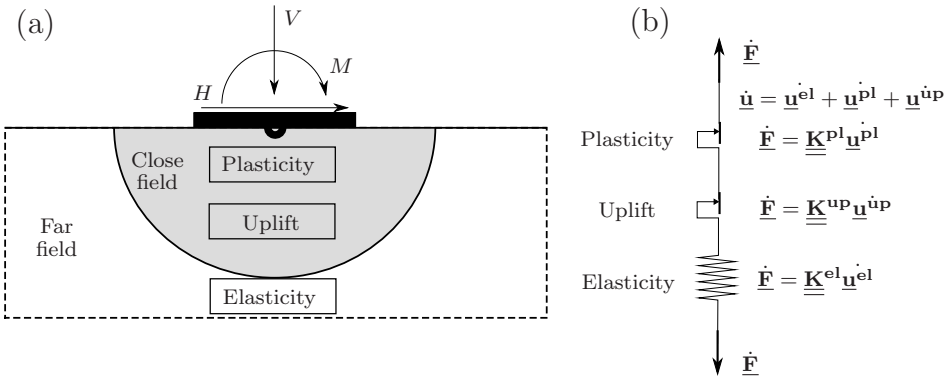

Fig. 1. Presentation of the general structure of the macro-element: (a) decomposition in close field and far field (b) analogical system.

2 Shape of the foundation and associated dimensionless variables

As usual is the case for a macro-element, it is appropriate to work with generalized (global) variables: the vertical force V, horizontal forces H_x, H_y and

moments M_x, M_y and the corresponding displacements, vertical settlement u_z, horizontal displacements u_x, u_y and rotations θ_x, θ_y. Torque moment (M_z) is not taken into account in the current version of the macro-element in order to facilitate the coupling with uplift. However, some recent plasticity models (single surface - isotropic hardening) have been extended to 6 degrees of freedom and calibrated with experiments, (Bienen et al., 2006). It would feasible to extend the macro-element following the same ideas. The displacement and force vectors are dimensionless and differ according to the shape (circular, rectangular and strip) of the foundation (in the following the symbol $'$ defines dimensionless variables).

For all the different types of foundations, the reduced forces are denoted as follows:

(i) Reduced horizontal forces: H'_x, H'_y
(ii) Reduced vertical force: V'
(iii) Reduced moments: M'_x, M'_y

and the reduced displacements are:

(i) Reduced horizontal displacements: u'_x, u'_y
(ii) Reduced vertical displacements
(iii) Reduced rotations: θ'_x, θ'_y

2.1 Circular footing

The generalized variables for a circular footing are given in figure 2. Their associate dimensionless variables are (see equations 1 and 3):

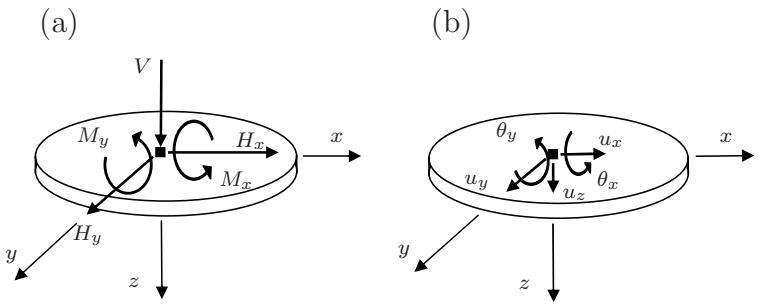

Fig. 2. Generalised variables: (a) forces and (b) displacements for a circular foundation.

$$\underline{\mathbf{F}} = \begin{bmatrix} V' \\ H'_x \\ M'_y \\ H'_y \\ M'_x \end{bmatrix} = \frac{1}{S q_{max}} \begin{bmatrix} V \\ H_x \\ M_y/D_{dm} \\ H_y \\ M_x/D_{dm} \end{bmatrix} \tag{1}$$

with D_{dm} the diameter and $S = (\pi D_{dm}^2)/4$ the surface area of the foundation. q_{max} is the ultimate compression stress of the soil under a vertical centred load (Davis et al., 1973), (Matar et al., 1979), (Philipponnat et al., 2003) but also (Randolph et al., 2004). For a circular footing it takes the following form:

$$q_{max} = \frac{0.6}{2}\gamma D_{dm} N_\gamma + q_0 N_q + 1.3 c N_c \tag{2}$$

where q_0 is the vertical effective stress at the bottom of the foundation, N_γ is the surface term, N_q a term depending on the depth of the foundation, and N_c the cohesion term. The relations allowing calculating N_γ,N_q and N_c are given in (Caquot et al., 1966) and (Randolph et al., 2004). They only depend on the cohesion c and the friction angle ϕ of the soil. The factors 0.6 and 1.3 are the shape factors of the coefficients N_γ,N_q and N_c for an axisymetric foundation.

In a similar way we obtain the displacements as follows:

$$\underline{\mathbf{u}} = \begin{bmatrix} u'_z \\ u'_x \\ \theta'_y \\ u'_y \\ \theta'_x \end{bmatrix} = \frac{1}{D_{dm}} \begin{bmatrix} u_z \\ u_x \\ D_{dm}\theta_y \\ u_y \\ D_{dm}\theta_x \end{bmatrix} \tag{3}$$

The right choice of the form of the vectors $\underline{\mathbf{F}}$ and $\underline{\mathbf{u}}$ is crucial. They are conjugated in order to calculate the work of forces applied to the foundation (Nova et al., 1991).

Following equations 1 and 3, the work of the reduced forces (W_r) for the normalized problem (according to the work of actual forces W_a) is provided by:

$$W_r = {}^t\underline{\mathbf{F}}.\underline{\mathbf{u}} = \frac{1}{D_{dm} S q_{max}} \left(V u_z + H_x u_x + M_y \theta_y + H_y u_y + M_x \theta_x\right)$$

$$= \frac{1}{D_{dm} S q_{max}} W_a \tag{4}$$

In other words, the real work is easily found by multiplying the work of the reduced forces by the constant factor $D_{dm} S q_{max}$.

2.2 Rectangular footing

For a rectangular $A \times B$ footing (figure 3), the following adimensinonal variables are proposed:

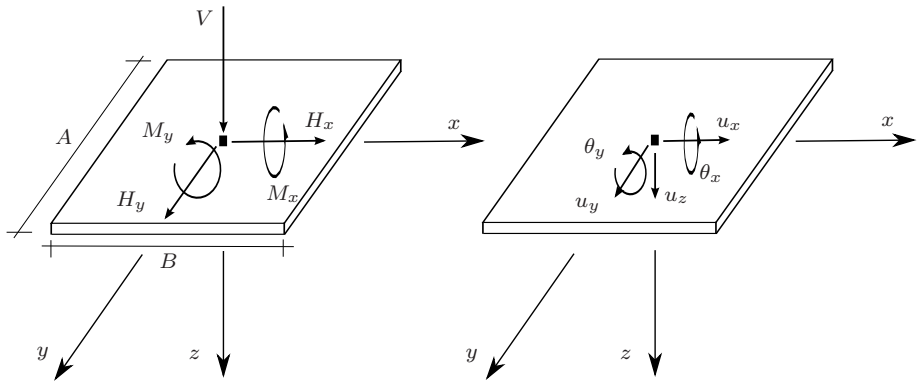

Fig. 3. Generalised variables: (a) forces and (b) displacements for a rectangular foundation.

$$\underline{\mathbf{F}} = \begin{bmatrix} V' \\ H'_x \\ M'_y \\ H'_y \\ M'_x \end{bmatrix} = \frac{1}{AB q_{max}} \begin{bmatrix} V \\ H_x \\ M_y/B \\ H_y \\ M_x/A \end{bmatrix} \quad and \quad \underline{\mathbf{u}} = \begin{bmatrix} u'_z \\ u'_x \\ \theta'_y \\ u'_y \\ \theta'_x \end{bmatrix} = \frac{\sqrt{A^2+B^2}}{AB} \begin{bmatrix} u_z \\ u_x \\ B\theta_y \\ u_y \\ A\theta_x \end{bmatrix} \tag{5}$$

where q_{max} is calculated as (expression valid for a rectangular foundation with A the bigger length) (Davis et al., 1973), (Matar et al., 1979) and (Philipponnat et al., 2003):

$$q_{max} = \frac{1}{2}\left(1 - 0.2\frac{B}{A}\right)\gamma B N_\gamma + q_0 N_q + \left(1 + 0.2\frac{B}{A}\right) c N_c \tag{6}$$

Reduced forces and displacements are again conjugated. The work of reduced forces for the normalised problem is this time provided by:

$$W_r =^t \underline{\mathbf{F}}.\underline{\mathbf{u}} = \frac{\sqrt{A^2+B^2}}{q_{max}(AB)^2}\left(V u_z + H_x u_x + M_y \theta_y + H_y u_y + M_x \theta_x\right)$$
$$= \frac{\sqrt{A^2+B^2}}{q_{max}(AB)^2} W_a \tag{7}$$

In other words, the real work is easily found by multiplying the work of the reduced forces by the constant factor $q_{max}(AB)^2/\sqrt{A^2+B^2}$.

In case where one of the two lengths (A or B) is very big, this normalisation is matching with the adimensional variables proposed in (Crémer et al., 2001) for a strip footing (see also section 2.3).

2.3 Strip footing

For a strip footing, it is more appropriate to use dimensionless variables given for one meter length of foundation (denoted with the foot script $_l$ symbol). For example, if the loading is in the plane (z, x), the vector $\underline{\mathbf{F}}$ takes the following form (Crémer et al., 2001):

$$\underline{\mathbf{F}} = \begin{bmatrix} V' \\ H'_x \\ M'_y \end{bmatrix} = \frac{1}{Bq_{max}} \begin{bmatrix} V/A \\ H_x/A \\ M_y/AB \end{bmatrix} = \frac{1}{Bq_{max}} \begin{bmatrix} V_l \\ H_{xl} \\ M_{yl}/B \end{bmatrix} \tag{8}$$

and

$$\underline{\mathbf{u}} = \begin{bmatrix} u'_z \\ u'_x \\ \theta'_y \end{bmatrix} = \frac{1}{B} \begin{bmatrix} u_z \\ u_x \\ B\theta_y \end{bmatrix} \tag{9}$$

The associated dimensionless vector $\underline{\mathbf{u}}$ is found by choosing a very big value for A.

Reduced forces and displacements are again conjugated. The work of reduced forces for the normalised problem is this time provided by:

$$W_r =^t \underline{\mathbf{F}}.\underline{\mathbf{u}} = \frac{1}{Bq_{max}}\left(V_l u_z + H_{xl} u_x + M_{yl}\theta_y\right) = \frac{1}{Bq_{max}} W_{a_l} \tag{10}$$

In other words, the real work is easily found by multiplying the work for one meter length of the reduced forces by the constant factor $1/Bq_{max}$.

3 Mathematical description of the macro-element

3.1 General remarks

The new SSI macro-element takes into account three different mechanisms: elasticity, plasticity of the soil and uplift of the foundation. The total displacement is thus decomposed as a sum of an elastic, plastic and uplift part:

$$\underline{\mathbf{u}} = \underline{\mathbf{u}}^{\mathbf{el}} + \underline{\mathbf{u}}^{\mathbf{pl}} + \underline{\mathbf{u}}^{\mathbf{up}} \tag{11}$$

Uplift is defined as the negative vertical displacement of the centre of the foundation. It is the result of rocking, i.e. the fact that the foundation rotates according to θ_x or θ_y (a part of the foundation looses contact with the soil), see figure 12. In order to compute uplift, the simple plasticity of the soil is not sufficient and a new non linear mechanism must be introduced. The reason is that the plasticity mechanism of the macro-element cannot take into account non linear geometrical effects (i.e. change of geometry of the foundation) which can lead to important negative vertical displacements ($u'_z < 0$). The uplift mechanism takes into account this change of geometry following a phenomelogical point of view. Another reason is that considering only the plasticity model there is not possible contraction of the plasticity surface.

Plasticity and uplift are strongly coupled (Crémer et al., 2001). More specifically:

(i) Plasticity and uplift mechanisms are taken into account according to the classical plasticity theory. They are described independently by failure criteria, loading surfaces, flow rules and hardening rules. Coupling of the two mechanisms is considered following the theory of multi-mechanisms.
(ii) 3D loadings can be studied, i.e. loadings according to the two horizontal and the vertical axis. As mentioned before, the torque moment M_x is not taken into account by the macro-element.

3.2 Elasticity mechanism

The elastic part of the constitutive law is defined in equation 12, where the displacement $\underline{\mathbf{u}}^{\mathbf{el}}$ and force vectors $\underline{\mathbf{F}}$ are dimensionless.

$$\underline{\mathbf{F}} = \underline{\underline{\mathbf{K}}}^{\mathbf{el}}\underline{\mathbf{u}}^{\mathbf{el}} = \underline{\underline{\mathbf{K}}}^{\mathbf{el}}\left(\underline{\mathbf{u}} - \underline{\mathbf{u}}^{\mathbf{pl}} - \underline{\mathbf{u}}^{\mathbf{up}}\right) \tag{12}$$

The elastic stiffness matrix $\underline{\underline{\mathbf{K}}}^{\mathbf{el}}$ is calculated using the real part of the static impedances (Grange et al., 2008a). It is considered diagonal, i.e. there is no coupling between the different directions of the loading. This is an important assumption that allows simplifying the problem. However, as other authors have showed the importance of the off-diagonal terms (Doherty et al., 2003), they could be introduced in a future version of the macro-element.

$$\underline{\underline{\mathbf{K}}}^{\mathbf{el}} = \begin{bmatrix} K'^{el}_{zz} & 0 & 0 & 0 & 0 \\ 0 & K'^{el}_{h_xh_x} & 0 & 0 & 0 \\ 0 & 0 & K'^{el}_{\theta_y\theta_y} & 0 & 0 \\ 0 & 0 & 0 & K'^{el}_{h_yh_y} & 0 \\ 0 & 0 & 0 & 0 & K'^{el}_{\theta_x\theta_x} \end{bmatrix} \tag{13}$$

With, for a circular footing:

$$\begin{cases} K'^{el}_{zz} = \frac{K^{el}_{zz} D}{S q_{max}} \\ K'^{el}_{h_xh_x} = K'^{el}_{h_yh_y} = K'^{el}_{hh} = \frac{K^{el}_{hh} D_{dm}}{S q_{max}} \\ K'^{el}_{\theta_y\theta_y} = K'^{el}_{\theta_x\theta_x} = K'^{el}_{\theta\theta} = \frac{K^{el}_{\theta\theta}}{D_{dm} S q_{max}} \end{cases} \tag{14}$$

For a rectangular footing:

$$\begin{cases} K'^{el}_{zz} = \frac{K^{el}_{zz}}{q_{max}\sqrt{A^2+B^2}} \\ K'^{el}_{h_xh_x} = K'^{el}_{h_yh_y} = \frac{K^{el}_{hh}}{q_{max}\sqrt{A^2+B^2}} \\ K'^{el}_{\theta_y\theta_y} = \frac{K^{el}_{\theta_y\theta_y}}{q_{max} B^2\sqrt{A^2+B^2}} \\ K'^{el}_{\theta_x\theta_x} = \frac{K^{el}_{\theta_x\theta_x}}{q_{max} A^2\sqrt{A^2+B^2}} \end{cases} \tag{15}$$

For a strip footing (with B the small dimension and A very big):

$$\begin{cases} K'^{el}_{zz} = \frac{K^{el}_{zz}}{q_{max}} \\ K'^{el}_{h_x h_x} = \frac{K^{el}_{h_x h_x}}{q_{max}} \\ K'^{el}_{\theta_y \theta_y} = \frac{K^{el}_{\theta_y \theta_y}}{B^2 q_{max}} \end{cases} \tag{16}$$

In the case of a strip footing, the others terms are not calculated.

The terms of this stiffness matrix are obtained using the real part of the static impedances defined in (Gazetas, 1991). The impedance represents the dynamic response of a zero-mass foundation lying on a semi-infinite soil considering its mass.

For a circular foundation:

$$\begin{cases} K_{hh} = \frac{4G_0 D}{2-\nu}\left(1 + 0.5\frac{D_{dm}}{2H}\right) \\ K_{zz} = \frac{2G_0 D}{1-\nu}\left(1 + 1.28\frac{D_{dm}}{2H}\right) \\ K_{\theta\theta} = \frac{G_0 D^3}{3(1-\nu)}\left(1 + 0.17\frac{D_{dm}}{2H}\right) \end{cases} \tag{17}$$

For a rectangular foundation we obtain (where $\beta_{h_x h_x}$, β_{zz} and $\beta_{\theta_y \theta_y}$ depend on the ratio $\frac{A}{B}$ and they are given in (Philipponnat et al., 2003)):

$$\begin{cases} K_{h_x h_x} = \frac{G_0}{1-\nu}\beta_{h_x h_x}\sqrt{AB} \\ K_{zz} = \frac{G_0}{1-\nu}\beta_{zz}\sqrt{AB} \\ K_{\theta_y \theta_y} = \frac{G_0}{1-\nu}\beta_{\theta_y \theta_y} b^2 \sqrt{AB} \end{cases} \tag{18}$$

For a strip footing the following relationships are provided in (Gazetas, 1991) (for a one meter length foundation):

$$\begin{cases} K_{h_x h_x} = \frac{2G_0}{2-\nu} \\ K_{zz} = \frac{0.73 G_0}{1-\nu} \\ K_{\theta_y \theta_y} = \frac{\pi G_0}{2(1-\nu)}\left(\frac{B}{2}\right)^2 \end{cases} \tag{19}$$

Equations 17, 18 and 19 depend on the geometrical properties of the foundation (diameter D_{dm}, or length A and B), the elastic stiffness properties of the soil (shear modulus G_0, Poisson ratio ν) and the depth H (measured from the surface) of the solid bed-rock.

3.3 Plasticity mechanism

The plasticity mechanism is briefly described hereafter. Detailed information can be found in (Grange et al., 2008a).

The failure criterion of the plasticity mechanism is defined for an overturning mechanism with uplift. It comes from (Pecker, 1997) and it has been used already in the 2D macro-element for a circular foundation presented in (Crémer et al., 2001).

The adaptation of the failure criterion in 3D and for different shapes comes from the following remark (see also (Grange et al., 2008a)): Expressing the failure surfaces found by different authors in the space of the dimensionless variables one can see that their form is rather similar (figure 4, where V_0 represents the bearing vertical capacity of the foundation). The adaptation in 3D consists thus on adding two more terms related with the horizontal force and moment in the other direction and assuming axial symmetry (equation 20).

$$f_\infty \equiv \left(\frac{H'_x}{aV'^c(1-V')^d}\right)^2 + \left(\frac{M'_y}{bV'^e(1-V')^f}\right)^2 + \left(\frac{H'_y}{aV'^c(1-V')^d}\right)^2 + \left(\frac{M'_x}{bV'^e(1-V')^f}\right)^2 - 1 = 0 \tag{20}$$

This is of course a rather harsh simplification but considering the nature of the macro-element and the level of precision that we want to obtain this first level of approximation is acceptable.

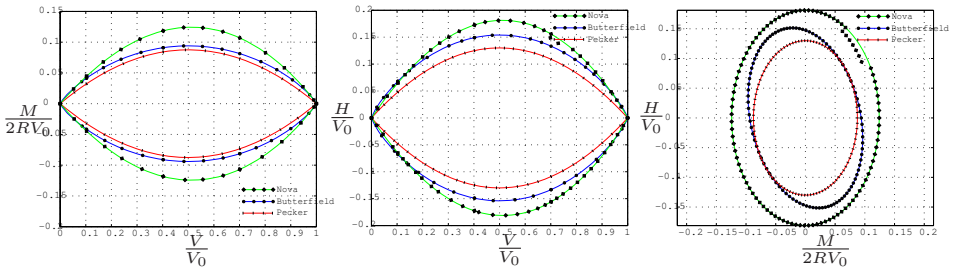

Fig. 4. Comparisons between the different failure surfaces given by several authors and plotted with adimensional variables. Strip foundations for (Nova et al., 1991) and (Pecker, 1997), circular for (Butterfield et al., 1994).

Following the same philosophy and for a 3D loading, the loading surfaces take the form (Grange et al., 2008a):

$$f_c\left(\underline{\mathbf{F}}, \underline{\tau}, \rho, \gamma\right) \equiv \left(\frac{H'_x}{\rho a V'^c (\gamma - V')^d} - \frac{\alpha}{\rho}\right)^2 + \left(\frac{M'_y}{\rho b V'^e (\gamma - V')^f} - \frac{\beta}{\rho}\right)^2 + \left(\frac{H'_y}{\rho a V'^c (\gamma - V')^d} - \frac{\delta}{\rho}\right)^2 + \left(\frac{M'_x}{\rho b V'^e (\gamma - V')^f} - \frac{\eta}{\rho}\right)^2 - 1 = 0 \tag{21}$$

The coefficients a, b define the size of the surface in the planes $(H' - M')$. c, d, e and f define the parabolic shape of the surface in the planes $(V' - M')$ and $(V' - H')$. Theses parameters can be fitted to different experimental results. For a semi-infinite space, the following values can be found in the literature (Crémer et al., 2001), table 1:

Table 1
Values of the loading surface parameters for a foundation lying on a semi-infinite space, (Crémer et al., 2001).

purely cohesive soil		purely frictional soil	
a	0.32	a	0.52
b	0.37	b	0.35
c	0.25	c	1
d	0.55	d	1
e	0.8	e	1
f	0.8	f	1

A representation of several loading surfaces at different step and the failure criterion is provided in figure 5. The denominators for the horizontal forces (the moments) are the same. Therefore, the interactions between the two horizontal forces (moments) are described by circles. It should be noted that equation 21 can not reproduce the eccentricity of Butterfield's experiments in the $H - M$ plane. This could be achieved if another $H - M$ coupled term is provided in the equation, (Houlsby et al., 2002).

$\underline{\tau} = [\alpha, \beta, \delta, \eta]$ is a vector composed of 4 kinematics hardening variables $\alpha, \beta, \delta, \eta$ and an isotropic hardening variable ρ. The variable γ is chosen to parametrize the second intersection point of the loading surface with the V' axis (the other point is the origin of the coordinate system) and its evolution on the same axis. The evolution of the hardening variables is obtained considering experimental results and numerical simulations (Crémer et al., 2001) of foundations under cyclic loadings. The mathematical expression of the failure criterion can be found by substituting $(\alpha, \beta, \delta, \eta, \rho, \gamma) = (0, 0, 0, 0, 1, 1)$ in equation 21.

An associate flow rule is considered in the $\left(H'_x, M'_y, H'_y, M'_x\right)$ hyperplane and non associated ones in the (H'_x, V'), $\left(M'_y, V'\right)$, $\left(H'_y, V'\right)$, (M'_x, V') planes (Grange

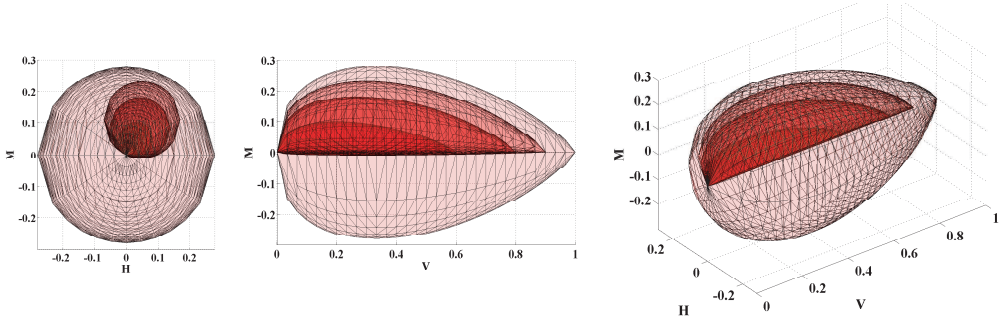

Fig. 5. Representation of the evolution of the loading surfaces within the failure criterion for a radial monotonic loading, in the $\left(H'_x - M'_y\right)$, $\left(M'_y - V'\right)$ planes and in the space $\left(H'_x - M'_y - V'\right)$.

et al., 2008a). A detailed description of the plasticity mechanism is given in (Grange et al., 2008a) and (Grange, 2008b).

3.4 Uplift mechanism

The mechanism presented hereafter describes in a phenomenological way uplift via a unique state variable δ. This variable represents the proportion of the surface of the uplifted footing (Crémer et al., 2001) (see also figure 6, D being the total length of the foundation). The macro-element being just a point, this is the only way to introduce the influence of the change of the geometry. We assume hereafter that uplift is not influenced by horizontal forces.

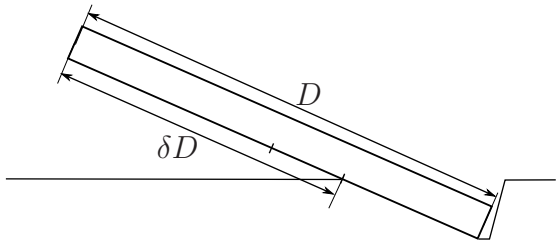

Fig. 6. Definition of δ, the proportion of the surface of the uplifted footing.

Figure 7 represents the 2D behaviour of a foundation on a plastic soil during uplift. One can identify the relation between $M' - \delta$ (M' being M'_x or M'_y), see also (Crémer et al., 2001). More specifically, the principal characteristics of this behaviour are:

- When the foundation undergoes a loading in one direction (for example $M' > 0$) the behaviour is elastic until the uplift initiation moment $M_0^{'(0)}$ is reached. After that point, the percentage of uplift δ increases creating uplift permanent displacements.

- During unloading ($\dot{M}' < 0$) the permanent displacements become visible (just like in a classical plasticity mechanism). The unloading slope ($\eta q_2/q_1$) is increased with respect to the original loading one (q_2/q_1) and δ decreases.
- Although the $M' - \delta$ unloading curve is linear (figure 7), the $M' - \theta^{up}$ curve is not linear (θ^{up} being the rotation due to uplift, see for example figures 10 and 11). Unloading does not follow an elastic linear behaviour and permanent displacements due to uplift can decrease.
- If a new loading cycle takes place, the behaviour can be at the beginning elastic till a new uplift initiation moment $M_0^{'(1)}$ is reached. The size of the elastic domain is thus found reduced.
- The two directions of loading ($M' > 0$ or $M' < 0$) are uncoupled. When the foundation undergoes a loading in the direction $M' > 0$ the other direction is not affected and the uplift initiation moment for $M' < 0$ remains unchanged.

q_1 and q_2 are shape factors. For a circular foundation $q_1 = 6$, $q_2 = 2$, for a rectangular-strip foundation $q_1 = 4$, $q_2 = 1$. The evolution of η is provided in equation 22, (Crémer et al., 2001):

$$\eta = 4 - 3e^{-4V'} \tag{22}$$

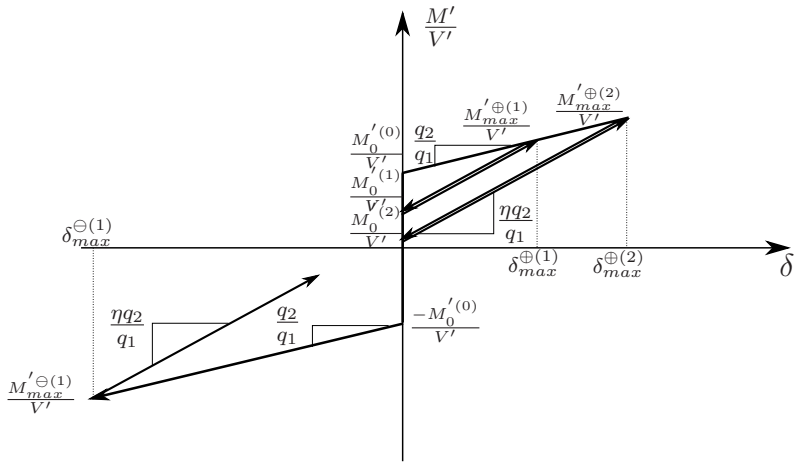

Fig. 7. Moment-δ relationship of a foundation on a plastic soil.

In order to robustly combine the non-linearities coming from the uplift mechanism with the ones coming from plasticity, the classical plasticity formalism is also chosen to describe uplift. This is presented in details hereafter:

3.4.1 Failure criterion

During uplift, failure occurs when the foundation is completely detached of the soil, in other words when $\delta = 1$. A simple analysis for different shapes of foundations (circular or rectangular or strip) lying on elastic soil allows finding the relation $M' = V'/2$ between the overturning moment and the

given vertical force. This equation can be actually considered as a failure criterion. On a plastic soil, the relationship between the overturning moment and the vertical force is more complicated (Crémer et al., 2001). Moreover, the overturning moment is linked with the shape of the foundation. For a loading in two different directions (for $M' > 0$ and $M' < 0$) we obtain (Grange, 2008b):

$$f_\infty \equiv M'^2 - \left(\frac{V'}{q_1}\left(e^{-AV'} + q_2\right)\right)^2 = 0 \tag{23}$$

where $A = 2.5$ is a dimensionless parameter.

3.4.2 Loading surfaces

During uplift, residual displacements can be generated at each part of the foundation combined with the plastification of the soil (see (Grange, 2008b) and figure 8). Furthermore, uplift is a non-linear, non reversible mechanism with the unloading slope increased with respect to the original loading one. The evolutions of the loading surfaces have thus to be activated even during unloading.

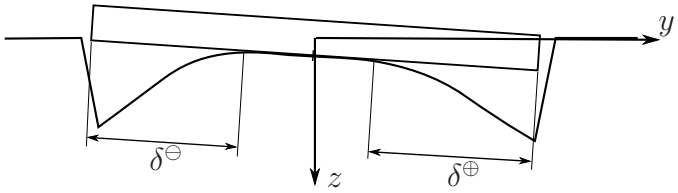

Fig. 8. Residual displacements on a plastic soil during uplift.

Figure 8 shows clearly the need to define two independent mechanisms for each directions of loading. Positive moments leads to uplift $\delta^\oplus$ and negative moments to uplift $\delta^\ominus$. The mathematical expressions of the loading surfaces for the directions $\oplus$ and $\ominus$ are provided in equation 24. In order to activate the loading surfaces in loading but also in unloading, they are chosen always positive whatever the sign of the loading.

$$\begin{cases} f^\oplus \equiv \left|M' - \frac{V'}{q_1}\left(e^{-AV'} + q_2\beta^\oplus\right)\right| = 0 \\ f^\ominus \equiv \left|M' + \frac{V'}{q_1}\left(e^{-AV'} - q_2\beta^\ominus\right)\right| = 0 \end{cases} \tag{24}$$

For the direction $\oplus$, the corresponding new hardening variable $\beta^\oplus$ evolves between δ and δ_{max} (maximal percent of uplift reached during the loading) and is defined as:

$$\beta^\oplus = \delta_{max}\left(1 - \eta\right) + \eta\delta \tag{25}$$

During an initial loading step, $\delta^{\oplus} = \delta^{\oplus}_{max}$ and thus $\beta^{\oplus} = \delta^{\oplus} = \beta^{\oplus}_{max} = \delta^{\oplus}_{max}$. It is only during unloading that $\beta^{\oplus}$ is different from $\delta^{\oplus}$. The same equations can be written for the other direction replacing $\oplus$ with $\ominus$.

3.4.3 Elastic zone

Unless the loading is important, an initial elastic domain exists. The mathematical expression of the surface defining the elastic limit zone is:

$$\begin{cases} f^{\oplus}_{el} \equiv M' - \frac{V'}{q_1} q_2 \beta^{\oplus(i)}_{max} (1-\eta) - \frac{V'}{q_1} e^{-AV'} = 0 \\ \\ f^{\ominus}_{el} \equiv M' - \frac{V'}{q_1} q_2 \beta^{\ominus(i)}_{max} (1-\eta) + \frac{V'}{q_1} e^{-AV'} = 0 \end{cases} \tag{26}$$

The loading surfaces being always positive, the following tests allow knowing which mechanism (elastic or uplift) is active:

$$\begin{cases} f^{\oplus}_{el}(M', V') \leq 0 \quad or \quad f^{\oplus}(M', V', \beta^{\oplus}) = 0 \quad \Rightarrow elasticity \\ f^{\oplus}_{el}(M', V') > 0 \quad and \quad f^{\oplus}(M', V', \beta^{\oplus}) > 0 \quad \Rightarrow uplift \end{cases} \tag{27}$$

The same equations are of course valid for the other direction replacing $\oplus$ with $\ominus$.

If residual uplift occurs on the $\oplus$ side of the foundation, the elastic domain entirely disappears. The mechanisms $\oplus$ and $\ominus$ can in principle be activated simultaneously. The graphical representation of all the surfaces is finally given in figure 9 at a given time t and is explained hereafter:

- In figure 9(a), the elastic domain still exists, the two mechanisms are not activated simultaneously. During this loading sequence the loading point is going through an elastic zone. One can nevertheless note that the size of the elastic domain has been reduced along the positive moments side of the graph $\oplus$. This behaviour is translated into figure 10 in terms of $M - \theta^{up}$, $M - u_z$ and $M - \delta^{\oplus} - \delta^{\ominus}$ relationships.
- In figure 9(b), the elastic domain does not exist any more, the two mechanisms are activated simultaneously and residual uplift displacements $\delta^{\oplus}$ and $\delta^{\ominus}$ subsist at each part of the foundation. During this loading sequence the loading point is not going through an elastic zone, the size of the elastic domain having vanished. This behaviour is translated into figure 11 in terms of $M - \theta^{up}$, $M - u_z$ and $M - \delta^{\oplus} - \delta^{\ominus}$ relationships.

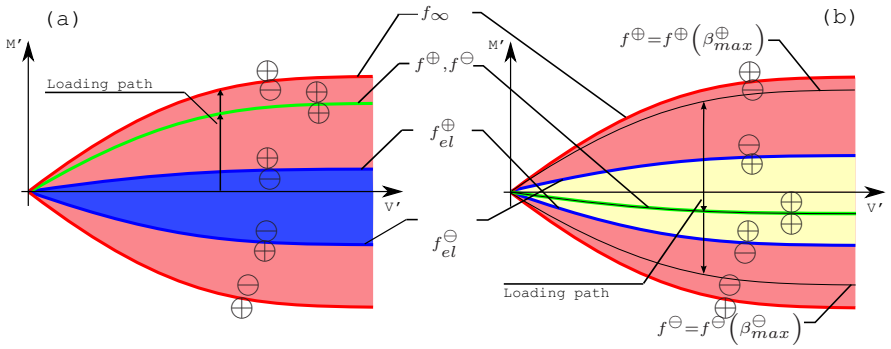

Fig. 9. Representation of the loading surfaces, failure criterion and elastic limits for uplift with their signs at a given time t.

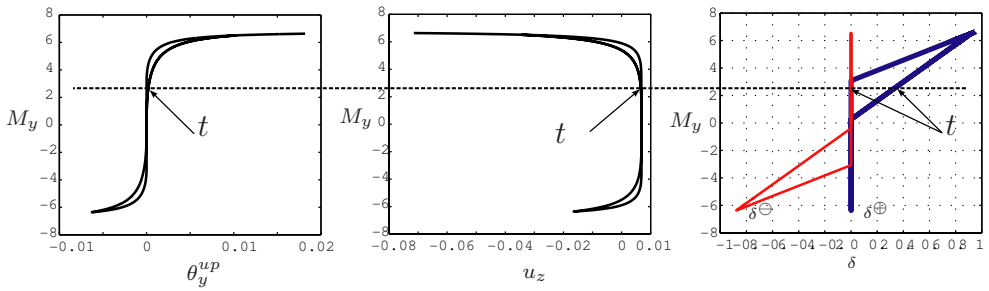

Fig. 10. Moment-rotation, moment-uplift, moment-δ relationships, case 1: existence of an elastic zone. t corresponds to the time step of figure 9(a).

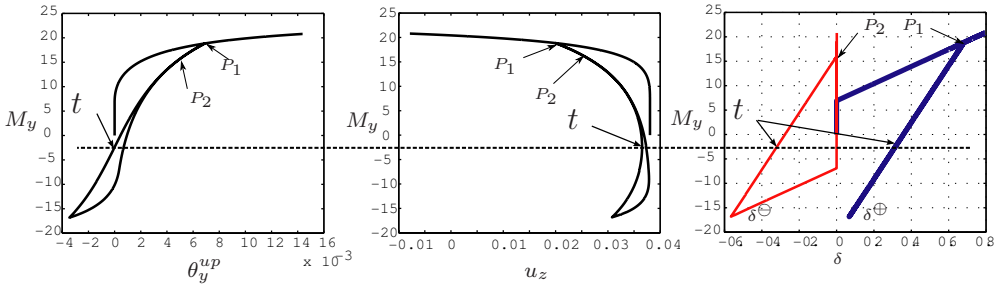

Fig. 11. Moment-rotation, moment-uplift, moment-δ relationships, case 2: no elastic zone. t corresponds to the time step of figure 9(b).

3.4.4 Kinematic hardening laws

While the loading point is situated outside the elastic domain, behaviour is non-linear during loading and unloading. Furthermore, displacements due to uplift decrease during unloading. The kinematic hardening laws have thus to be activated while on the monotonic loading curve and for loading-unloading.

This is done with the following equation (presented here for the $\oplus$ direction):

$$\begin{cases} \dot{\beta}^{\oplus} = \dfrac{\dot{\theta}'^{up}}{\theta'_0} \dfrac{\left(1-\beta^{\oplus}\right)^2}{\beta^{\oplus}(2-\beta^{\oplus})} \quad if \ \beta^{\oplus}=\beta^{\oplus}_{max} \ (monotonic \ loading \ curve) \\ \dot{\beta}^{\oplus} = \dfrac{\dot{\theta}'^{up}}{\theta'_0} \eta \dfrac{\left(1-\left(\frac{\beta^{\oplus}-(1-\eta)\beta^{\oplus}_{max}}{\eta}\right)\right)^2}{\frac{\beta^{\oplus}-(1-\eta)\beta^{\oplus}_{max}}{\eta}\left(2-\left(\frac{\beta^{\oplus}-(1-\eta)\beta^{\oplus}_{max}}{\eta}\right)\right)} \quad if \ \beta^{\oplus}\leq\beta^{\oplus}_{max} \ (loading-unload) \end{cases} \tag{28}$$

3.4.5 Flow rule

The flow rule is found through geometrical considerations, assuming that the centre of rotation of the foundation stays always at the middle of the non-uplifted segment (figure 12, (Grange, 2008b)). The uplift vertical displacement generated by the uplift rotation is given as follows:.

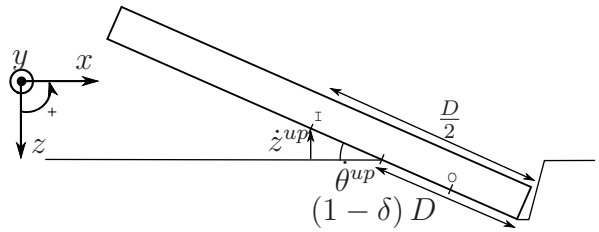

Fig. 12. Kinematics of a foundation for the uplift mechanism.

$$dz^{up} = -\left(\frac{D}{2} - \frac{D\,(1-\delta)}{2}\right) d\theta^{up} = -\frac{D\delta}{2} d\theta^{up} \tag{29}$$

Equation 29 leads to the velocity (without dimension):

$$\dot{z}'^{up} = -\frac{\delta}{2}\dot{\theta}'^{up} \tag{30}$$

As the uplift mechanism does not generate any other displacements (e.g. horizontal displacements), the flow rule is completely described by equation 31.

$$\frac{\partial g}{\partial V'} = -\frac{\delta}{2}\frac{\partial g}{\partial M'} \tag{31}$$

A new function f_g is introduced to define the sign of the term $\frac{\partial g}{\partial M'}$ considering that:

- $\frac{\partial g}{\partial M'} \geq 0$ if the loading point moves from inside to outside the loading surface f (figure 9);
- $\frac{\partial g}{\partial M'} \leq 0$ if the loading point moves from outside to inside the loading surface f.

f_g is built from the function f with the difference that f_g is only positive outside and negative inside. It is calculated as:

$$f_g \equiv M^{'2} - \frac{V^{'2}}{q_1}\left(1 + q_2\left|\delta\right|\right) = 0 \tag{32}$$

The following equations finally link the uplift rotation and the uplift vertical displacement of the foundation:

$$\begin{cases} \frac{\partial g}{\partial M'} = \frac{f_g}{|f_g|} = sign(f_g) \\ \frac{\partial g}{\partial V'} = -\frac{\delta}{2}\frac{f_g}{|f_g|} = -\frac{\delta}{2}sign(f_g) \end{cases} \tag{33}$$

3.5 3D behaviour

For a 3D loading, a simplified way to model uplift is to define uplift mechanisms in two horizontal directions similar to the mechanism presented before. The mechanisms are then coupled considering a projection in the principal direction of solicitations ((Grange, 2008b), figure 13).

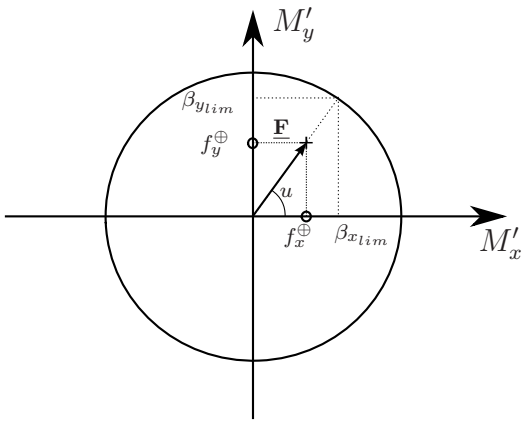

Fig. 13. Uplift kinematic for a circular foundation, loading direction estimation to evaluate the limits of the uplift kinematic variables.

The loading surfaces, elastic zones and failure criteria of the two mechanisms are presented hereafter (where u is the angle defining the principal direction of the solicitation).

For the direction x:

$$\begin{cases} f_{x_{el}}^{\oplus} \equiv M' - \frac{V'}{q_1} q_2 \beta_{x_{max}}^{\oplus(i)} (1-\eta) - \frac{V'}{q_1} e^{-AV'} |\cos u| = 0 \\ f_x^{\oplus} \equiv \left| M' - \frac{V'}{q_1} \left(e^{-AV'} |\cos u| + q_2 \beta_x^{\oplus} \right) \right| = 0 \\ f_{x_{el}}^{\ominus} \equiv M' - \frac{V'}{q_1} q_2 \beta_{x_{max}}^{\ominus(i)} (1-\eta) + \frac{V'}{q_1} e^{-AV'} |\cos u| = 0 \\ f_x^{\ominus} \equiv \left| M' + \frac{V'}{q_1} \left(e^{-AV'} |\cos u| - q_2 \beta_x^{\ominus} \right) \right| = 0 \\ f_{x_\infty} \equiv M'^2 - \left(\frac{V'}{q_1} \left(e^{-AV'} |\cos u| + q_2 \right) \right)^2 = 0 \end{cases} \tag{34}$$

For the direction y:

$$\begin{cases} f_{y_{el}}^{\oplus} \equiv M' - \frac{V'}{q_1} q_2 \beta_{y_{max}}^{\oplus(i)} (1-\eta) - \frac{V'}{q_1} e^{-AV'} |\sin u| = 0 \\ f_y^{\oplus} \equiv \left| M' - \frac{V'}{q_1} \left(e^{-AV'} |\sin u| + q_2 \beta_y^{\oplus} \right) \right| = 0 \\ f_{y_{el}}^{\ominus} \equiv M' - \frac{V'}{q_1} q_2 \beta_{y_{max}}^{\ominus(i)} (1-\eta) + \frac{V'}{q_1} e^{-AV'} |\sin u| = 0 \\ f_y^{\ominus} \equiv \left| M' + \frac{V'}{q_1} \left(e^{-AV'} |\sin u| - q_2 \beta_y^{\ominus} \right) \right| = 0 \\ f_{y_\infty} \equiv M'^2 - \left(\frac{V'}{q_1} \left(e^{-AV'} |\sin u| + q_2 \right) \right)^2 = 0 \end{cases} \tag{35}$$

Considering that the hardening variables of the two uplift mechanisms should tend respectively to $\beta_{x_{lim}} = |\cos u|$ and $\beta_{y_{lim}} = |\sin u|$, they are calculated as follows (see also equation 28):

For the $\oplus$ mechanism:

$$\begin{cases} \dot{\beta}_x^{\oplus} = \frac{\dot{\theta}_x'^{up}}{\theta_0'} \frac{\left(\beta_{x_{lim}} - \beta_x^{\oplus} \right)^2}{\beta_x^{\oplus} \left(2\beta_{x_{lim}} - \beta_x^{\oplus} \right)} \quad if \ \ \beta_x^{\oplus} = \beta_{x_{max}}^{\oplus(i)} (monotonic \ \ loading \ \ curve) \\ \dot{\beta}_x^{\oplus} = \frac{\dot{\theta}_x'^{up}}{\theta_0'} \eta \frac{\left(\beta_{x_{lim}} - \left(\frac{\beta_x^{\oplus} - (1-\eta)\beta_{x_{max}}^{\oplus(i)}}{\eta} \right) \right)^2}{\frac{\beta_x^{\oplus} - (1-\eta)\beta_{x_{max}}^{\oplus(i)}}{\eta} \left(2\beta_{x_{lim}} - \left(\frac{\beta_x^{\oplus} - (1-\eta)\beta_{x_{max}}^{\oplus(i)}}{\eta} \right) \right)} \quad if \ \ \beta_x^{\oplus} \leq \beta_{x_{max}}^{\oplus(i)} (load-unload) \end{cases} \tag{36}$$

For the $\ominus$ mechanism:

$$\begin{cases} \dot{\beta}_x^{\ominus} = \frac{\dot{\theta}_x'^{up}}{\theta_0'} \frac{\left(\beta_{x_{lim}} + \beta_x^{\ominus} \right)^2}{-\beta_x^{\ominus} \left(2\beta_{x_{lim}} + \beta_x^{\ominus} \right)} \quad if \ \ \beta_x^{\ominus} = \beta_{x_{max}}^{\ominus(i)} (monotonic \ \ loading \ \ curve) \\ \dot{\beta}_x^{\ominus} = \frac{\dot{\theta}_x'^{up}}{\theta_0'} \eta \frac{\left(\beta_{x_{lim}} + \left(\frac{\beta_x^{\ominus} - (1-\eta)\beta_{x_{max}}^{\ominus(i)}}{\eta} \right) \right)^2}{-\frac{\beta_x^{\ominus} - (1-\eta)\beta_{x_{max}}^{\ominus(i)}}{\eta} \left(2\beta_{x_{lim}} + \left(\frac{\beta_x^{\ominus} - (1-\eta)\beta_{x_{max}}^{\ominus(i)}}{\eta} \right) \right)} \quad if \ \ \beta_x^{\ominus} \geq \beta_{x_{max}}^{\ominus(i)} (load-unload) \end{cases} \tag{37}$$

The same equations are obtained for the direction y by replacing x by y.

Remark 1:

With this formalism, if $\beta^{\oplus}$, $\beta^{\ominus}$ are the "fictive" hardening variables in the principal direction of loading, the following equations are every time verified:

$$\begin{cases} \beta_x^{\oplus} = \beta_{x_{lim}} \beta^{\oplus} \\ \beta_x^{\ominus} = \beta_{x_{lim}} \beta^{\ominus} \\ \beta_y^{\oplus} = \beta_{y_{lim}} \beta^{\oplus} \\ \beta_y^{\ominus} = \beta_{y_{lim}} \beta^{\ominus} \end{cases} \tag{38}$$

Remark 2:

In this problem, two uplift variables are calculated (the first along the direction x and the second along the direction y). Is there a risk to generate too high vertical displacements? The answer is no because the two hardening variables tend respectively to $\beta_{x_{lim}}$ and $\beta_{y_{lim}}$.

The demonstration follows:

Let's consider a radial loading resulting to a rotation θ_u. $\delta_u \in [0, 1]$ is the corresponding percentage of uplift. The decomposition of the uplift rotation into the coordinate system of the foundation is:

$$\begin{cases} \theta_x'^{up} = |\cos u| \, \theta_u'^{up} \\ \theta_y'^{up} = |\sin u| \, \theta_u'^{up} \end{cases} \tag{39}$$

The vertical displacement is calculated thanks to the flow rule defined for the uplift mechanism (equation 30). For each direction we obtain:

$$\begin{cases} u_z'^{up^x} = -\frac{\delta_x}{2} \theta_x'^{up} \\ \\ u_z'^{up^y} = -\frac{\delta_y}{2} \theta_y'^{up} \end{cases} \tag{40}$$

Therefore, the total uplift generated by the two mechanisms is:

$$u_z'^{up^{tot}} = u_z'^{up^x} + u_z'^{up^y} \tag{41}$$

Furthermore, at each step the uplift variables verify:

$$\begin{cases} \delta_x = |\cos u|\, \delta_u \\ \delta_y = |\sin u|\, \delta_u \end{cases} \tag{42}$$

By introducing equations 39, 40, 42 into equation 41 we obtain (because $|\cos u|^2 + |\sin u|^2 = 1$):

$$u_z^{'up^{tot}} = -\frac{\delta_u}{2}\theta_u^{'up} \tag{43}$$

4 Coupling of the two non-linear mechanisms: plasticity and uplift

Coupling of the plasticity and uplift mechanisms is done following the classical theory of multi-mechanisms (Simo et al., 1998), (Grange, 2008b). A representation of the superposition of the different surfaces is given in figure 14.

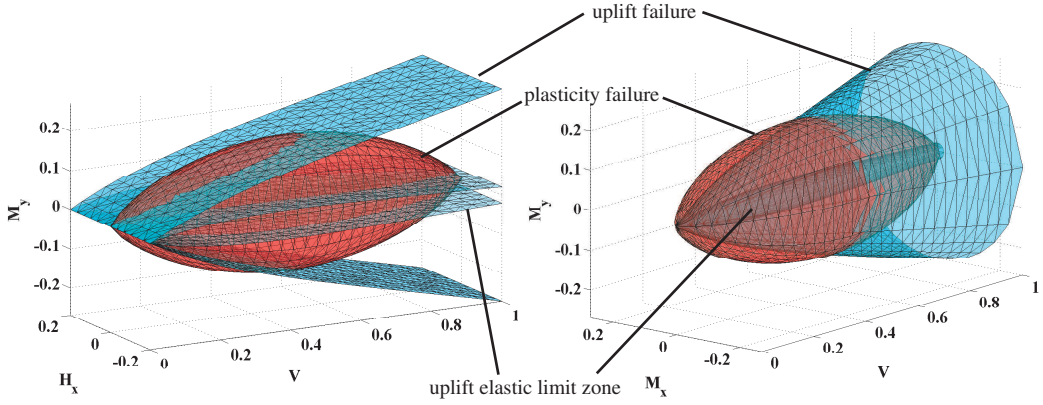

Fig. 14. Representation of the failure criterion and of the initial elastic limit zone for the uplift mechanism (blue) and the failure criterion for the plasticity mechanism (red) in the spaces M_y, H_x, V and M_y, M_x, V.

In practice there are not two but five mechanisms to link: the plasticity mechanism and the two uplift mechanisms ($\oplus$ and $\ominus$) for each direction (x and y). Each mechanism generates residual displacements. Let's define $\underline{\mathbf{u}}^{\mathbf{pl}^m}$ the contribution of a mechanism m with $m \in [1, M]$ and with $M \in [1, 5]$ the number of the activated mechanism. The total plastic velocity can thus be written as follows:

$$\underline{\dot{\mathbf{u}}}^{\mathbf{pl}} = \sum_{m=1}^{M} \underline{\dot{\mathbf{u}}}^{\mathbf{pl}^m} \tag{44}$$

Due to the normality rule we have:

$$\underline{\dot{\mathbf{u}}}^{\mathbf{pl}} = \sum_{m=1}^{M} \dot{\lambda}^m \frac{\partial g^m}{\partial \underline{\mathbf{F}}} \tag{45}$$

Let's also define $f^1\left(\underline{\mathbf{F}}, \underline{\mathbf{q}}^1\right)$, $f^2\left(\underline{\mathbf{F}}, \underline{\mathbf{q}}^2\right)$, $f^3\left(\underline{\mathbf{F}}, \underline{\mathbf{q}}^3\right)$, $f^4\left(\underline{\mathbf{F}}, \underline{\mathbf{q}}^4\right)$ and $f^5\left(\underline{\mathbf{F}}, \underline{\mathbf{q}}^5\right)$ the loading surfaces of the five mechanisms. $\underline{\mathbf{F}}$ represents the loading vector and $\underline{q}^m$ represents the hardening variable array of the mechanism m.

Following the classical plasticity theory the Kuhn-Tucker conditions have to be verified:

$$\dot{\lambda}^m \geq 0 \quad f^m \leq 0 \quad \dot{\lambda}^m f^m = 0 \tag{46}$$

The consistency condition is checked for each mechanism in order to calculate the corresponding plastic potential $\lambda^m, m \in [1, M]$. This condition translates the fact that the loading point has always to be on the loading surfaces. In other words, for the mechanism m, the relationships $\dot{f}^m = 0$ and $f^m = 0$, $m \in [1, M]$ have always to be checked.

The first condition allows calculating the plastic multiplier (considering that $\underline{\dot{\mathbf{F}}} = \underline{\underline{\mathbf{K}}}^{\mathbf{el}}\left(\underline{\dot{\mathbf{u}}} - \underline{\mathbf{u}}^{\dot{\mathbf{up}}}\right)$) as follows :

$$\begin{aligned} \dot{f}^i = 0 &\Leftrightarrow \frac{\partial f^i}{\partial \underline{\mathbf{F}}} \cdot \underline{\dot{\mathbf{F}}} + \sum_{j=1}^{M} \frac{\partial f^j}{\partial \underline{\mathbf{q}}_{\mathbf{j}}^{\mathbf{pl}}} \cdot \underline{\dot{\mathbf{q}}}_{\mathbf{j}}^{\mathbf{pl}} = 0 \\ &\Leftrightarrow \frac{\partial f^i}{\partial \underline{\mathbf{F}}} \cdot \underline{\underline{\mathbf{K}}}^{\mathbf{el}} \underline{\dot{\mathbf{u}}} - \sum_{j=1}^{M} \dot{\lambda}^i \frac{\partial f^j}{\partial \underline{\mathbf{F}}} \cdot \underline{\underline{\mathbf{K}}}^{\mathbf{el}} \frac{\partial g^j}{\partial \underline{\mathbf{F}}} - \dot{\lambda}^j \frac{\partial f^j}{\partial \underline{\mathbf{q}}_{\mathbf{j}}^{\mathbf{pl}}} \cdot \underline{\mathbf{h}}_{\mathbf{j}}^{\mathbf{pl}} = 0 \end{aligned} \tag{47}$$

The previous M equations are coupled and the plastic multipliers $\dot{\lambda}^i$ are given hereafter:

$$\begin{bmatrix} \dot{\lambda}^1 \\ \dot{\lambda}^2 \\ \vdots \\ \dot{\lambda}^M \end{bmatrix} = \left[\underline{\underline{\mathbf{H}}}^{\mathbf{pl}} + \underline{\underline{\mathbf{H}}}_{\mathbf{0}}^{\mathbf{pl}}\right]^{-1} \begin{bmatrix} \frac{\partial f^1}{\partial \underline{\mathbf{F}}} \cdot \underline{\underline{\mathbf{K}}}^{\mathbf{el}} \underline{\dot{\mathbf{u}}} \\ \frac{\partial f^2}{\partial \underline{\mathbf{F}}} \cdot \underline{\underline{\mathbf{K}}}^{\mathbf{el}} \underline{\dot{\mathbf{u}}} \\ \vdots \\ \frac{\partial f^M}{\partial \underline{\mathbf{F}}} \cdot \underline{\underline{\mathbf{K}}}^{\mathbf{el}} \underline{\dot{\mathbf{u}}} \end{bmatrix} \tag{48}$$

where $\underline{\underline{\mathbf{H}}}^{\mathbf{pl}}$ is the diagonal matrix of plastic multiplier $H_{ij}^{pl} = \delta_i^j \frac{\partial f^i}{\partial \underline{\mathbf{q}}_{\mathbf{i}}^{\mathbf{pl}}} \cdot \underline{\mathbf{h}}_{\mathbf{j}}^{\mathbf{pl}}$ without sum according to i and δ_i^j the Kronecker δ. $\underline{\underline{\mathbf{H}}}_{\mathbf{0}}^{\mathbf{pl}}$ is the matrix defined

by the terms $H_{0_{ij}}^{pl} = \frac{\partial f^i}{\partial \underline{\mathbf{F}}} \cdot \underline{\underline{\mathbf{K}}}^{\mathbf{el}} \frac{\partial g^j}{\partial \underline{\mathbf{F}}}$.

If we consider

$$\underline{\underline{\mathbf{H}}}_{\mathbf{T}} = \left[\underline{\underline{\mathbf{H}}}^{\mathbf{pl}} + \underline{\underline{\mathbf{H}}}_{\mathbf{0}}^{\mathbf{pl}}\right]^{-1} \tag{49}$$

we finally obtain for M coupled mechanisms:

$$\dot{\underline{\mathbf{F}}} = \underbrace{\left(\underline{\underline{\mathbf{K}}}^{\mathbf{el}} - \sum_{i=1}^{M}\sum_{j=1}^{M} H_{T_{ij}} \left(\underline{\underline{\mathbf{K}}}^{\mathbf{el}} : \frac{\partial g^i}{\partial \underline{\mathbf{F}}}\right) \otimes \left(\frac{\partial f^j}{\partial \underline{\mathbf{F}}} : \underline{\underline{\mathbf{K}}}^{\mathbf{el}}\right)\right)}_{\underline{\underline{\mathbf{K}}}^{\mathbf{elpl}}} \dot{\underline{\mathbf{u}}} \tag{50}$$

The macro-element is implemented into FEDEASLab, a finite element Matlab toolbox (Filippou et al., 2004). The return mapping algorithm (Simo et al., 1998) is used for the plasticity and uplift mechanisms.

5 TRISEE: Experimental campaign and numerical simulations

The numerical performance of the macro-element and the influence of plasticity and uplift on the behaviour of a rectangular foundation are studied hereafter using the experimental results of the European program TRISEE (TRISEE, 1998).

5.1 Experimental set-up and loading

Within the European program TRISEE, several experiments were performed on a shallow rectangular foundation lying on a Low Density sand (LD) sand and a High Density sand (HD) (TRISEE, 1998). Horizontal cyclic solicitations were applied at the top of a vertical beam resting on the foundation, while a vertical force was kept constant throughout the tests (figure 15). More specifically:

- The dimensions of the foundation were $1m$ x $1m$.
- The vertical beam was $0.9m$ high.
- The dimensions of the sand box were $4.6m$ x $4m$ x $4m$.
- The constant vertical force V was equal to $100kN$ for the LD sand and $300kN$ for the HD sand.
- The horizontal cyclic solicitations were divided in three phases:

(1) Phase I, small sine-shaped horizontal force cycles.

(2) Phase II, pseudo-dynamic force solicitation representative of a seismic loading.
(3) Phase III, sine-shaped horizontal displacement cycles of increasing amplitude.

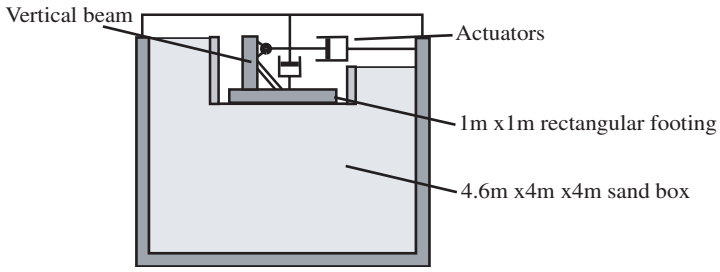

Fig. 15. TRISEE: experimental set-up.

5.2 Numerical model

The new SSI macro-element able to couple plasticity and uplift is used to simulate the foundation. An elastic beam reproduces the upper structure. The node at the base of the macro-element is considered fixed, whereas the horizontal and vertical loadings are applied at the upper end of the elastic beam.

The parameters of the numerical model are presented in table 2 and 3. They have been calibrated using the experimental moment-rotation and horizontal force-horizontal displacement diagrams. They are divided into two groups:

(1) The ones that change between the three phases (table 2). During the different experimental phases the soil actually settled something that led to an increase of the ultimate bearing capacity of the foundation and to a decrease of the elastic stiffnesses particularly in rotation. A curve showing the decrease of the elastic parameters at the beginning of the different phases is provided into (TRISEE, 1998). Based on this experimental evidence we have tuned numerically the initial elastic stiffness for the different phases.
(2) The ones that stay constant during the three phases (table 3). The coefficients of the loading surface presented in table 3 have been chosen in order to fit the the experimental curves and particularly the position of their horizontal plateaux. They are different from the ones provided in table 1, which are valid for a semi infinite soil (Crémer et al., 2001). This shows clearly that the assumption of semi infinite soil cannot be applied in this case and that is difficult to obtain a priori the right values for a cohesive or a frictional soil.

Table 2
TRISEE: Non constant parameters of the numerical model.

Phase	HD	LD
I	$K_{\theta\theta}^{el} = 52MNm/rad$	$K_{\theta\theta}^{el} = 25MNm/rad$
	$K_{hh}^{el} = 105MN/m$	$K_{hh}^{el} = 45MN/m$
	$K_{zz}^{el} = 120MN/m$	$K_{zz}^{el} = 65MN/m$
	$q_{max} = 0.58MPa$	$q_{max} = 0.14MPa$
II	$K_{\theta\theta}^{el} = 52MNm/rad$	$K_{\theta\theta}^{el} = 15MNm/rad$
	$K_{hh}^{el} = 105MN/m$	$K_{hh}^{el} = 35MN/m$
	$K_{zz}^{el} = 120MN/m$	$K_{zz}^{el} = 40MN/m$
	$q_{max} = 0.58MPa$	$q_{max} = 0.14MPa$
III	$K_{\theta\theta}^{el} = 35MNm/rad$	$K_{\theta\theta}^{el} = 5MNm/rad$
	$K_{hh}^{el} = 75MN/m$	$K_{hh}^{el} = 14MN/m$
	$K_{zz}^{el} = 80MN/m$	$K_{zz}^{el} = 26.6MN/m$
	$q_{max} = 1.5MPa$	$q_{max} = 0.185MPa$

Table 3
TRISEE: Constant parameters of the numerical model.

Plasticity parameters	HD	LD	Plasticity parameters	HD	LD
a	0.93	1.1	κ	1	1
b	0.8	0.9	ξ	1	1
c	1	0.8	a_1	1	1
d	1	0.8	a_2	1	1
e	1	0.8	a_3	1	1
f	1	0.8	a_4	1	1
			a_5	1	1

5.3 Experimental vs. Numerical results

Numerical and experimental results for the phases I, II and III and for the LD and HD sands are given in figures 16, 17 and 18. We present each time the moment-rotation, horizontal force-displacement and vertical displacement-time curves.

5.3.1 Phase I

Figure 16 shows the behaviour of the foundation on the LD and HD sands during phase I. This phase generates only small non-linearities. The numerical model reproduces correctly the behaviour of the foundation in terms of horizontal displacements and rocking angles (which are slightly underestimated). Important differences appear however on the vertical displacements. A possible explanation could the fact that Phase I is actually a "set-up" phase for the foundation on the soil whereas the amplitude of the load is small.

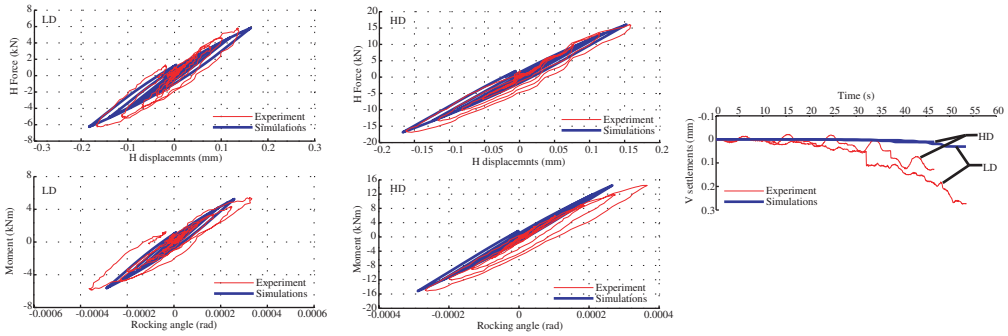

Fig. 16. TRISEE: Phase I, experimental and numerical results for the LD and HD sands.

5.3.2 Phase II

Figure 17 shows the behaviour of the foundation on the LD and HD sands during phase II. Plasticity is now more pronounced. The loops of the force-displacement relationships are wide-opened and vertical settlements become important (of the order of centimetre). It can be also noted that no uplift occurs during this phase.

Numerical results are again satisfactory in terms of horizontal displacements and rocking angles in both directions. The size of the loops is correctly reproduced, indicating that the model dissipates energy in a similar manner than the experiment. Finally, it is also important to notice that vertical displacements are well reproduced by the macro-element, particularly for the LD sand.

Note: For the LD case, due to numerical reasons, we applied displacements and not forces on the top of the beam.

5.3.3 Phase III

Figure 18 shows the behaviour of the foundation on the LD and HD sands for phase III. Important non-linearities are developed during this displacement

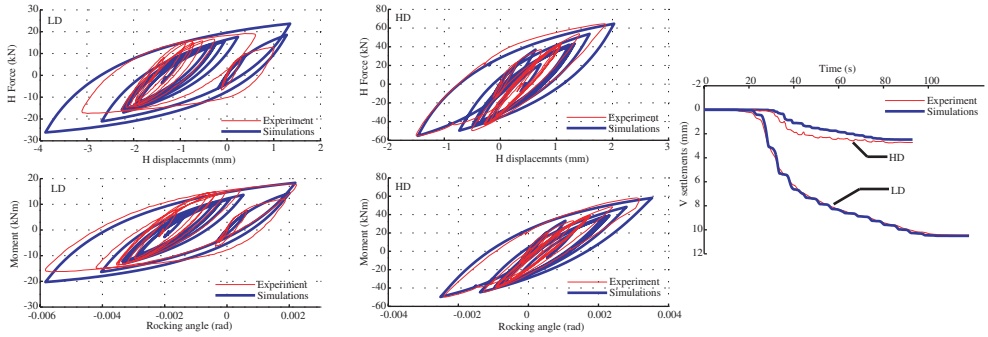

Fig. 17. TRISEE: Phase II, experimental and numerical results for the LD and HD sands.

controlled phase. As can be seen from the S-shaped curve, the influence of uplift is important for the HD sand. For the LD sand instead, only plasticity is developed and the vertical settlements are important. The experimental horizontal force - displacement curve shifts towards the negative direction of the horizontal displacements although the loading and the geometry of the mock-up are symmetric.

Except for the non symmetric curve, numerical results reproduce satisfactory the behaviour of the foundation in terms of horizontal forces and moments in both directions. For the LD case, the model generates more plasticity (bigger loops) than the experiment, something that can explain the higher numerical vertical settlements. For the HD case, the model reproduces correctly the influence of uplift (S-shaped curve).

In order to quantify the influence of uplift, we proceed to the same calculation deactivating the uplift components of the macro-element, see figure 19. One can clearly identify the influence of uplift looking at the S-shaped moment-rotation curve for the HD sand. Rotations due to the plasticity of the soil are found almost equal to the ones coming from uplift. In other words, uplift and plasticity of the soil have similar contributions on the moment-rocking angle curve for the HD sand. Finally another interesting remark is that if uplift is not taken into account, the waves present on the settlement curve are not reproduced (HD case).

6 Conclusions

The 3D SSI macro-element developed within this work is able to simulate the non linear behaviour of shallow rigid foundations of circular, rectangular of strip shape on an infinite space submitted to cyclic loadings. It takes into account the plasticity of the soil and the uplift of the foundation. Using global variables it has the advantage of inducing low computational costs (couple of

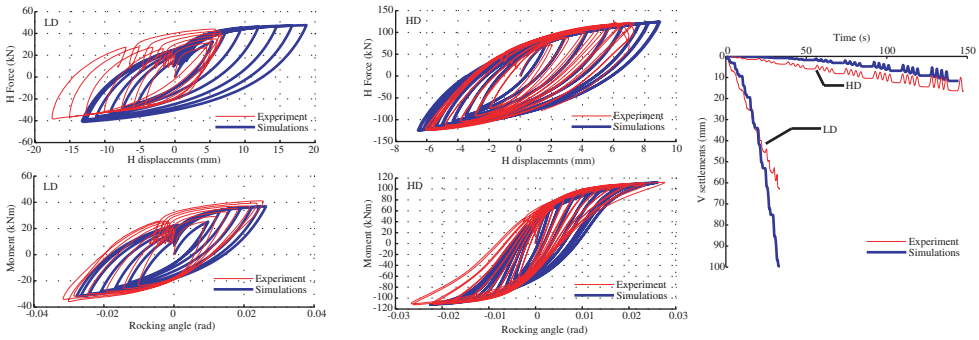

Fig. 18. TRISEE: Phase III, experimental and numerical results for the LD and HD sands.

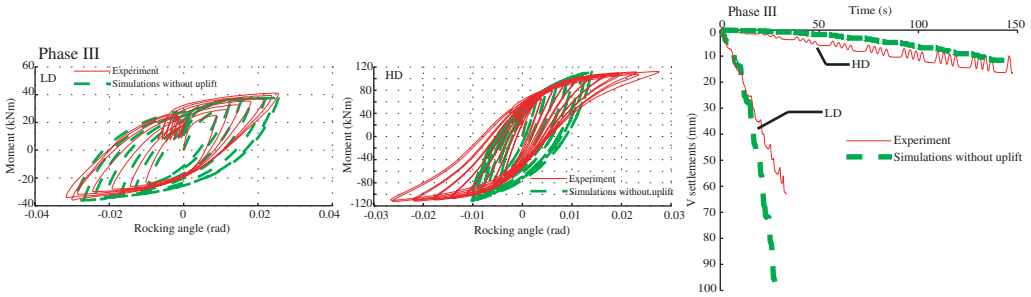

Fig. 19. TRISEE: Phase III, importance of the uplift. Numerical results are presented considering only the plasticity mechanism (the uplift mechanism is deactivated) for the LD and HD sands.

minutes for each simulation).

The paper presents the three mechanisms considered in the macro-element (elasticity, plasticity and uplift) and their coupling. Uplift is formulated using the classical plasticity theory. The numerical performance of the element is finally validated using the experimental results of the European program TRISEE.

An interesting result coming from the numerical validation of the macro-element is that for a foundation on a high density sand, rotations due to the plasticity of the soil can be equal to the ones coming from uplift. In other words, uplift and plasticity of the soil can have similar contributions on the moment-rocking angle curve. Furthermore, the uplift mechanism is necessary in order to reproduce the waves often present on the time - settlement curve. It is obvious that in certain cases uplift has significant influence on the behaviour of a foundation and thus it can not be neglected.

The 3D behaviour of the element has not yet been validated due to the difficulty to find experimental results with loadings in 2 horizontal directions. This point should constitute the subject of a future work.

Acknowledgements

The authors are grateful for the financial support of the European Contract LESSLOSS, Risk Mitigation for Earthquakes and Landslides of the Sixth Framework Programme (Project No.: GOCE-CT-2003-505488).

References

Bienen, B., Byrne, B.W., Houlsby, G.T., Cassidy, M.J., 2006. Investigating six degree of freedom loading of shallow foundations on sand. *Géotechnique*; **56**(6):367–379.

Butterfield, R., Gottardi, G., 1994 A complete three-dimensional failure envelope for shallow footings on sand *Géotechnique*; **44**(1):181–184.

Caquot, A., Kérisel, J., 1966 *Traité de mécanique des sols,* Gautiers-Villars, France.

Cassidy, M.J., Byrne, B.W., Houlsby, G.T., 2002 Modelling the behaviour of circular footings under combined loading on loose carbonate sand. *Géotechnique*; **52**(10):705–712.

Crémer, C., Pecker, A., Davenne, L., 2001 Cyclic macro-element for soil-structure interaction: material and geometrical non-linearities. *International Journal for Numerical and Analytical Methods in Geomechanics*; **25**(13):1257–1284.

Crémer, C., Pecker, A., Davenne, L., 2002 Modelling of nonlinear dynamic behaviour of a shallow strip foundation with macro-element. *Journal of Earthquake Engineering*; **6**(2):175–211.

Crémer, C., Pecker, A., Davenne, L., 2002 Modelling of nonlinear dynamic behaviour of a shallow strip foundation with macro-element. *Journal of Earthquake Engineering*; **6**(2):175–211.

Davis, E.H., Booker, J.R., 1973 The effect of increasing strength with depth on the bearing capacity of clays. *Géotechnique*; **23**(4):551–563.

di Prisco, C., Nova, R., Sibilia, A., 2002 *Analysis of soil-structure interaction of towers under cyclic loading.* invited lecture, Proc. NUMOG 8, Rome, G.N.Pande & S. Pietruszczak editors, Swets & Zeitlinger, Lisse, 637–642.

di Prisco, C., Galli, A., 2006 *Mechanical behaviour of shallow foundations under cyclic loads.* ALERT Workshop 2006 (without proceedings), Technical University (Politecnico) of Milan Italy.

Doherty, J.P., Deeks, A.J., 2003 Elastic response of circular footings embedded in a non-homogeneous half-space. *Géotechnique*; **53**(8):703–714.

Filippou, F.C., Constandines, M., 2004 *FedeasLab Getting Started Guide And Simulations Examples.* Department of Civil and Environmental Engineering UC Berkeley.

Gazetas, G., 1991 *Foundations vibrations.* Foundation Engineering Handbook, Chapter 15. Fang H-Y (ed.), van Nostrand Reinhold: New York.

Grange, S., Kotronis, P., Mazars, J., 2008 A macro-element for a circular foundation to simulate 3D soil-structure interaction. *International Journal for Numerical and Analytical Methods in Geomechanics*; **32**(10):1205–1227.

Grange, S., 2008 *Modélisation simplifiée 3D de l'interaction sol-structure: application au génie parasismique.* PhD Thesis, laboratoire 3S-R, INP Grenoble, France, http://tel.archives-ouvertes.fr/tel-00306842/fr/

Houlsby, G.T., Cassidy, M.J., 2002 *A plasticity model for the behaviour of footings on sand under combined loading. Gotechnique* **52, No. 2**:117–129.

Martin, C.M., 1994 *Physical and numerical modelling of offshore foundations under combined loads.* DPhil Thesis, University of Oxford.

Matar, M., Salençon, J., 1979 Capacité portante des semelles filantes. *Revue française de Géotechnique*; **9**:51–76.

Nova, R., Montrasio, L., 1991 Settlements of shallow foundations on sand. *Géotechnique*; **41**(2):243–256.

Montrasio, L., Nova, R., 1997 Settlements of shallow foundations on sand: geometrical effects *Géotechnique*; **47**(1):49–60.

Paolucci, R., Pecker, A., 1997 Seismic bearing capacity of shallow strip foundations on dry soils. *Soils and Foundations, Japanese Geotechnical Society*; **37**(3):95–105.

Pecker, A., 1997 Analytical formulae for the seismic bearing capacity of shallow strip foundations. In *Seismic Behavior of Ground and Geotechnical Structures,* Seco e Pinto (ed.). Balkema: Rotterdam; 261–268.

Pedretti, S., 1998 *Nonlinear seismic soil-foundation interaction: analysis and modelling method.* PhD thesis, Dpt Ing Strutturale, Politecnico di Milano.

Philipponnat, G., Hubert, B., 2003 *Fondations et ouvrages en terre,* Eyrolles, Paris, France.

Randolph, M.F., Jamiolkowski, M.B., Zdravkovi, L., 2004. Load carrying capacity of foundations. *Proc. Skempton Memorial Conf., London*; **1**:207–240.

Simo, J.C., Hughes, T.J.R., 1998 *Computational Inelasticity,* Mechanics and materials, Springer Interdisciplinary applied mathematics, vol.7.

Tan, F.S.C., 1990 *Centrifuge and theoretical modelling of conical footings on sand.* PhD thesis, University of Cambridge.

TRISEE, 1998, 3D Site Effects and Soil-Foundation Interaction in Earthquake and vibration Risk Evaluation, Part 4 *Large-scale geotechnical experiments on soil-foundation interaction.* European Commission, Directorate General XII for science, Research and Development.